Determination of strength of UG2 chromitite pillars at Impala Platinum from laboratory tests and FLAC3D

by B.P. Watson, T.J. Maphosa, D.P. Roberts, and L.J. Gardner

Affiliation:
University of the Witwatersrand, Johannesburg, South Africa

Correspondence to:
B.P. Watson

Email:
bryan.watson@wits.ac.za

Dates:
Received: 26 Jan. 2024
Revised: 23 May 2024
Accepted: 19 Jun. 2024
Published: August 2024

How to cite:
Watson, B.P., Maphosa, T.J., Roberts, D.P., and Gardner, L.J. 2024. Determination of strength of UG2 chromitite pillars at Impala Platinum from laboratory tests and FLAC3D. *Journal of the Southern African Institute of Mining and Metallurgy*, vol. 124, no. 8. pp. 437–446

DOI ID:
http://dx.doi.org/10.17159/2411-9717/3261/2024

ORCID:
B.P. Watson
http://orcid.org/0000-0003-0787-8767
T.J. Maphosa
http://orcid.org/0000-0003-3114-7198
D.P. Roberts
http://orcid.org/0000-0002-7517-4836

Abstract

The results of FLAC3D modelling on chromitite Upper Group 2 Reef pillars from the Bushveld Complex of South Africa are described. The model input parameters were determined from laboratory triaxial tests with post-failure measurements. These geomechanical tests were performed on rock materials within the pillars and the immediate pillar foundations. In the models, post-failure behaviour was simulated using the concept of cohesion softening. Models were built to determine the strength and behaviour of pillars with a width-to-height ratio of approximately two. The original research aimed to find a suitable depth below the surface where Impala Platinum Ltd could safely introduce crush pillars; however, the paper only describes the model results: the ideal depth of the crush pillar introduction is not discussed. The results of the modelling are compared with the PlatMine formula for peak pillar strength and with an underground instrumented pillar located elsewhere on the same reef. Some insight into the effects of grid size on strength is also provided. Further underground measurements are recommended to verify the model results.

Keywords

pillar strength; laboratory rock tests; FLAC3D; modelling parameters, post-failure, machine stiffness, crush pillars

Introduction

The project described in this paper was carried out to determine the depth below the surface at which 4 m × 2 m crush pillars can be safely implemented in the conventional sections of the Upper Group 2 (UG2) reef at the Impala Platinum Rustenburg Operations (Impala). The expected mining height of these sections is 1.3 m. This paper describes the laboratory tests and numerical modelling that were done to achieve the objective. In particular, the pillar behaviour and strengths that were established by the modelling are described, but the ideal depth of crush pillar introduction is not discussed.

A series of geomechanical compression tests were conducted at various levels of confinement in the Gold Fields test laboratory at the University of the Witwatersrand. The aim of these tests was to determine the pre- and post-peak behaviour of the 'reef' rock types, as well as the immediate footwall and hangingwall rocks. FLAC3D modelling input parameters were determined from these tests, which, in turn, were used to simulate the pillar behaviour and determine the peak and residual strengths of the pillars.

The Impala operations are located in the Western Lobe of the Bushveld Complex. The mining operation is situated 30 km north of Rustenburg, in the Northwest Province of South Africa (Figure 1).

The Bushveld Complex is comprised of a series of shallow-dipping layers of chromitite, pyroxenite, norite, and anorthosite (Impala Mine Rock Engineering Department, 2017). At the Impala operations, these layers have an average dip of 9° towards the northeast (Impala Mine Rock Engineering Department, 2017). Two platinum-bearing orebodies are currently being mined, namely: Merensky Reef and UG2 Reef.

Most of the mining at the Impala operations is carried out using conventional labour-intensive stoping on a scattered basis, which allows for selective mining with geological losses left unmined. The regional support strategy comprises regularly spaced barrier pillars together with geological losses. In the stopes, pillar support consists of non-yielding pillars, yield pillars, and crush pillars (Impala Mine Rock Engineering Department, 2017). Figure 2 shows the typical stress–strain behaviour of in-stope pillars (Ryder and Jager, 2002). Points Y and C marked in Figure 2 indicate the operating points of yield and crush pillars, respectively.

Crush pillars offer the advantage of improving the extraction ratio and pose no pillar burst risk at their residual strength. However, pillars of crush pillar size can be susceptible to violent failure if they do not fail

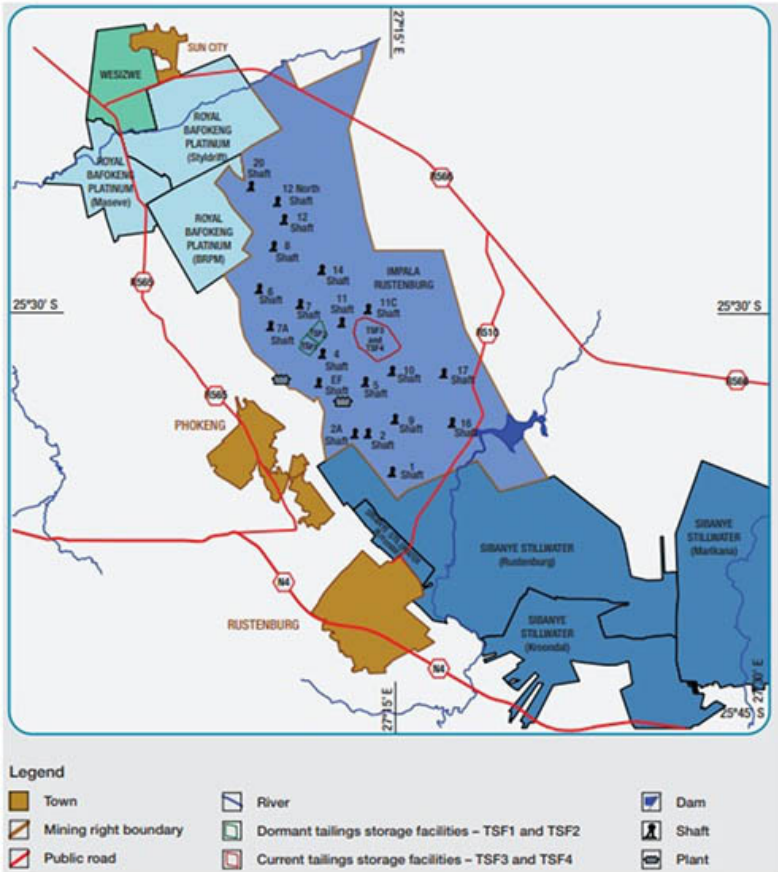

Figure 1—Location of Impala operations (McLachlan, 2021)

close to the face (Watson, 2010; Watson et al., 2010). To prevent this, the stress at the face must surpass the peak strength of the pillar; otherwise crushing will not occur and the pillar becomes a hazard in the back area (Du Plessis, 2015).

The residual strength of the pillar determines how much weight the crushed pillars can carry (Watson et al., 2010). Therefore, it is crucial to estimate both the peak and residual strength of the pillar to ensure it can perform according to the design. Typically, this estimation involves costly underground measurements. This study concentrated on the UG2 reef because most research conducted on Bushveld pillars to date has focused on the Merensky pillars.

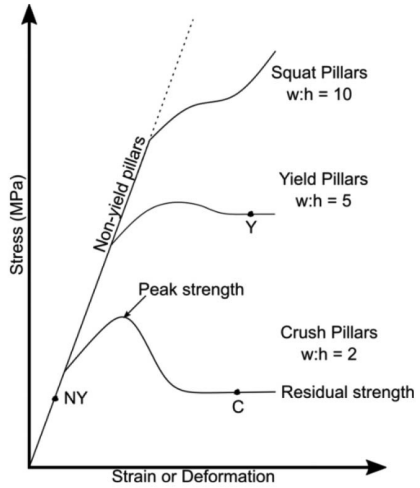

Figure 2—Typical in-stope pillar stress–strain behaviour (after Ryder and Jager, 2002)

Literature review

Implications of test machine stiffness on rock test

According to Hudson et al. (1972), a testing machine is characterized as either soft or stiff for a given rock specimen. During testing, both the specimen and the machine deform as the load increases (Salamon, 1970). Salamon (1970) observed that the equilibrium between the testing machine and the sample remains stable if the machine is unable to induce further displacement in the specimen without a supply of additional external energy. This is in line with observations made by Cook (1963), which led him to conclude that the violent brittle behaviour observed during testing was due to excess energy stored in the machine. This resulted in the design of stiff testing machines. To obtain a complete stress–strain curve, the following condition must be met throughout the test to avoid abrupt violent failure (Hudson et al., 1972):

$$\text{Stiffness of the machine} > \text{post-peak stiffness of the sample} \quad [1]$$

Rock specimen behaviour

Class I post-peak behaviour

Rocks that exhibit Class I behaviour require work to be done on them to induce further deformation (Wawersik and Fairhurst, 1970). Fracture propagation is stable, provided that the highest absolute value of post-peak stiffness is less than the machine stiffness (Hudson et al., 1972). Typical Class I behaviour of rock means that both the axial and lateral strain continuously increase during the deformation cycle (Oniyide, 2015).

Figure 3 shows a typical Class I stress–strain curve, with shaded regions indicating energy supplied by the testing machine and energy required to deform the rock specimen (Vogler, 2014). Additional energy would have to be supplied by the machine to continue testing from point A to point B in Figure 3. The shaded area (1 + 2 + 3) represents the energy supplied by the machine from point O to point B. The energy supplied by the machine to reach the peak at point A is represented by area (1 + 2). Area (1) represents the non-recoverable energy, including the energy required for crack formation, crack propagation, plastic deformation, heat, extension, etc.

Area (2) shows the elastic energy stored in the sample at point A. The additional energy required to deform the rock sample from point A to point B is represented by Area (3). If the testing machine has sufficient stiffness, i.e., the unloading curve of the machine is equivalent or steeper than that of the rock sample, it is possible to trace out the complete stress–strain curve for Class I rock samples (Vogler, 2014).

Class II post-peak behaviour

Class II behaviour is characterized by unstable and self-sustaining fracture propagation. To obtain a complete stress–strain curve, energy must be extracted from the sample being tested (Vogler, 2014). Machine stiffness on its own is not adequate to control the failure of a Class II rock type (Vogler, 2014). A servo-controlled mechanism is required to back off the loading platens during fracture propagation. Lateral strain is used as the control measurement under these conditions (during the immediate pre- and post-peak phase), as it is the only variable that monotonically increases throughout the rock test (Oniyide, 2015).

Figure 4 shows a typical Class II stress–strain curve, with shaded regions indicating energy supplied by the testing machine and energy required to be removed from the rock specimen immediately after failure (Vogler, 2014). In Figure 4, the axial strain increases from point O to point A, then decreases from point A to point B, after which it starts to increase again until point C. Area (1 + 2 + 4) represents the total energy supplied by the machine to deform the rock specimen. The energy supplied by the machine to reach peak strength is represented by area (1 + 2 + 3). Area (3) represents the energy that needs to be extracted from a Class II rock sample in post-peak. Area (1) shows the non-recoverable energy. Areas (2 + 3) show the elastic energy present in the sample at point A. The energy required to complete the test from peak strength (from point A to point C) is represented by area (2 + 4) (Vogler, 2014).

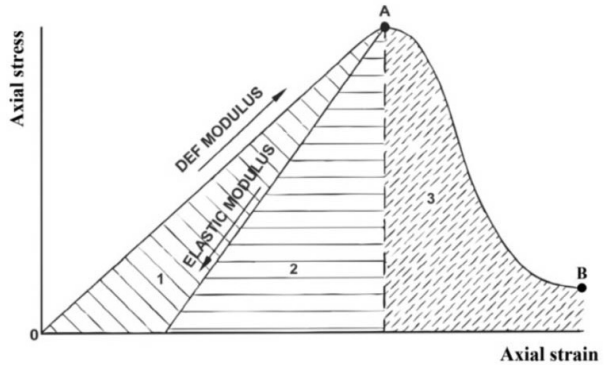

Figure 3—Typical Class I behaviour (Vogler, 2014). Area 1 represents the non-recoverable energy; Area 2 shows the elastic energy stored in the sample at point A; Area 3 represents the additional energy required to deform the rock sample from point A to point B

Crush pillars

Crush pillars are slender pillars with a width/height (w/h) ratio < 3; they are designed to fail close to the face under stiff loading conditions. The pillars retain some strength after failure, known as residual strength (Ozbay et al., 1995). This residual strength is used to support the immediate hangingwall to prevent back breaks (Watson, 2009). They are typically used from 600 m below the surface, but can be used at shallower depths with caution (Ozbay et al., 1995). At shallower depths, they become susceptible to violent failure when the available stress at the face is too low to fail the pillar (Watson, 2010). The residual strength supports the immediate hangingwall up to the highest active parting plane, making it crucial to ensure sufficient residual strength.

Numerical simulations

FLAC3D was used in conjunction with the Mohr–Coulomb model with strain softening (Hajiabdolmajid et al., 2002) because of its proven ability to account for post-peak behaviour. An Itasca constitutive Model for Advanced Strain Softening (IMASS) has been developed (Itasca, 2023). The literature on IMASS (Itasca, 2023; Ghazvinian et al., 2020) shows the response for only one pillar, which displays characteristics that can be replicated using the Mohr–Coulomb strain-softening (MCSS) model. There was therefore no apparent advantage to using the IMASS model for modelling pillar responses, particularly given the many prior examples of successful application of the MCSS model (Watson et al., 2008; Malan and Napier, 2011; Le Bron et al., 2024).

The Hoek–Brown failure criterion was not used in the models because it provides limited softening behaviour and has not been shown to simulate the post-peak behaviour of pillars (Itasca, 2023). Significant effort was, however, expended to ensure that there was parity between calibrated Hoek–Brown and Mohr–Coulomb parameters.

Laboratory testing

Geomechanical tests and results

More than 50 cylindrical rock specimens with length/width ratios of 2.5 were prepared according to the International Society for Rock Mechanics (ISRM) specifications, as described by Ulusay and Hudson (2007). Three triaxial compressive strength (TCS) tests were conducted at confinement levels of 10 MPa, 20 MPa, and 40 MPa for each of the three rock types. Oil leakage occurred at 40 MPa

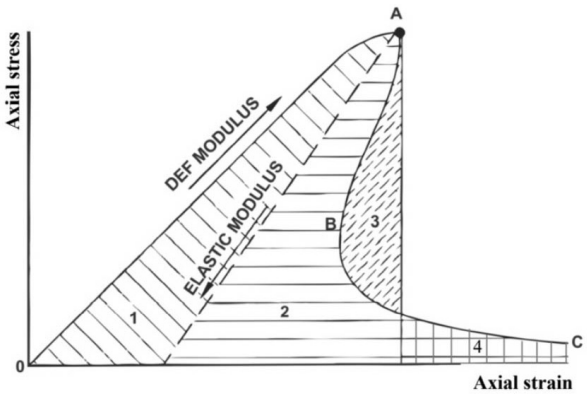

Figure 4—Typical Class II behaviour (Vogler, 2014). Area 1 shows the non-recoverable energy; Areas 2 and 3 show the elastic energy present in the sample at point A. The energy required to complete the test from peak strength (A–C) is shown by area (2 + 4)

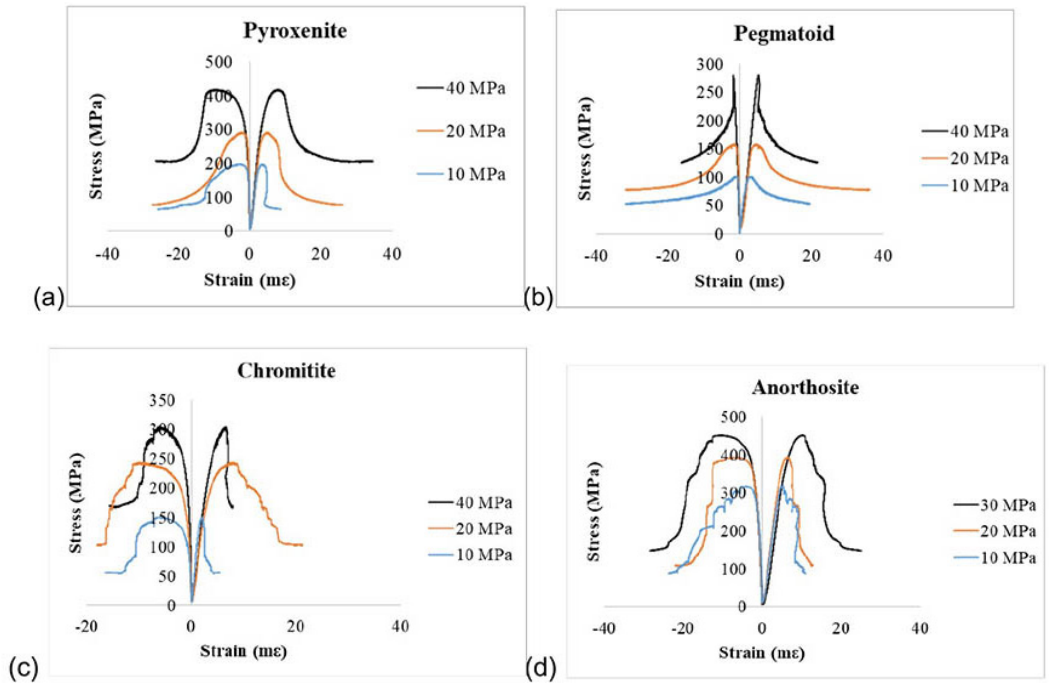

Figure 5—Stress-strain curves for (a) pyroxenite, (b) pegmatoid, (c) chromitite, and (d) anorthosite

in the anorthosite samples, so the maximum confinement in this rock type was limited to 30 MPa. The tests were carried out using a servo-controlled stiff testing machine (MTS 815) to allow for the monitoring of post-failure behaviour. Unconfined compressive strength (UCS) tests were also conducted, but no post-failure deformations were measured in these tests.

Triaxial compressive strength test results

Examples of the TCS test results are provided in Figure 5. The anorthosite and pyroxenite rock types were sourced from the immediate footwall and hangingwall of the pillars, respectively. They both demonstrated transitional behaviour between Class I and Class II post-failure behaviour at confinement levels of 10 MPa and 20 MPa. At higher confinements, these rock types exhibited Class I behaviour. Interestingly, the pegmatoid and chromitite samples showed Class I behaviour at 10 MPa and 20 MPa, and transitional behaviour at 40 MPa. Further testing should be done to confirm these behaviour patterns.

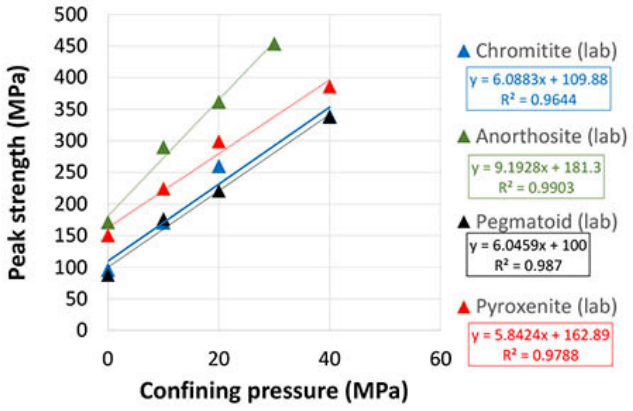

Figure 6—Plot of peak strength as a function of confining pressure

Test data analysis

In Figure 6, the average peak strength results from the TCS and UCS tests are plotted as a function of confining stress. A linear regression with a coefficient of fit is provided for each rock type. The test results from the Impala database (Gardner and Bosman, 2014) provided similar peak strength results.

The residual strength of each rock type was taken as the constant strength that the rock retains after failure. The residual strength is similarly influenced by confinement to the peak strength. Figure 7 illustrates the effect of confinement on the average residual strength of the various rock types. The graph demonstrates that the residual strength rises with higher confining stress as a linear function.

The cohesion and friction angle were determined using Equations [2] and [3] (Jaeger and Cook, 1979), respectively:

$$\emptyset = \sin^{-1}\left(\frac{m-1}{m+1}\right)\sigma_c; \qquad [2]$$

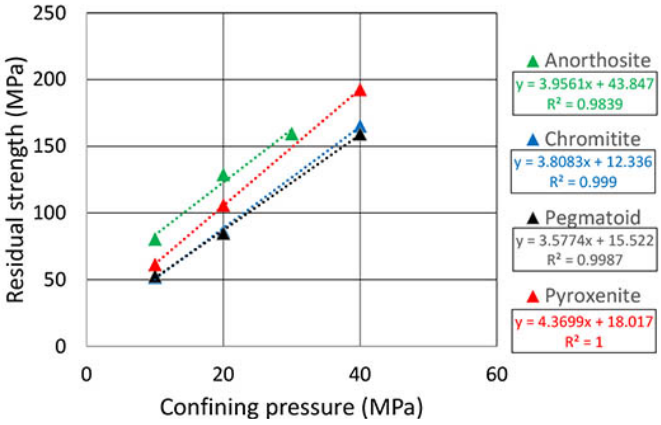

Figure 7—Effect of confinement on residual strength

$$C = \left(\frac{1-\sin\emptyset}{\cos\emptyset}\right)\sigma_c\,, \qquad [3]$$

where σ_c is the UCS of the rock type, m is the strengthening parameter (gradient) shown in Figures 6 and 7, c is the cohesion of intact rock, and Φ is the internal friction angle.

Crush pillar model

The results of the rock tests were downrated to account for the rock mass by using the geological strength index (GSI), as described by Hoek (1994). Rock mass values of cohesion and friction were determined by using the RocLab software program (2007). Impala considers a GSI value of 60 to provide a reasonable description of the rock mass conditions across the mine (Gardner, 2022). The disturbance factor (*D*), to account for blasting damage, was originally set at 0.3 (Oniyide, 2015), but it was found that there was only a marginal difference of about 3 MPa in peak strength between *D*-values of 0.3 and zero. The FLAC3D (Itasca, 2023) models were therefore run using the laboratory-determined parameters, downrated by RocLab (2007) (using a GSI of 60) with *D* set to zero. These results were then compared with models that were run without downrating or data manipulation. The models were set up using a built-in structured hexahedral grid generation.

The pillar dimensions in the model were 4 m × 2 m and 1.3 m high, and the stope span between pillars was 30 m, as provided by the mine. The hangingwall and footwall thicknesses were 5 m and 4.8 m, respectively, as shown in Figure 8. A 1.5 m holing was cut every 4 m to ensure 4 m long pillars, and gully dimensions of 1.3 m wide and 1.8 m deep were also included (Carollo, 2022), as shown in Figure 9. The constitutive model was set to the maximum Coulomb shear stress (MCSS) criterion, based on the cohesion-weakening model (Hajiabdolmajid et al., 2002). Roller boundaries were applied to the model sides and base, to simulate repeating geometries along both axes. A velocity of 10^{-6} m/s was applied to the top of the model, and the average pillar stress was calculated across the centre height of the pillar.

Figure 9 shows the modelled area in plan view, with shaded rectangles representing the crush pillars modelled for two scenarios. Scenario 1 had a 2 m siding between the pillar and the gully and Scenario 2 had no siding. Both scenarios assumed zero dips to simplify the model. The plastic strain input parameters were estimated by analysing FLAC3D models of the laboratory triaxial tests and back-fitting the stress–strain curves obtained from these tests. An example is provided in Figure 10.

The final input values of cohesion, dilation angle, and friction angle are provided as a function of plastic shear strain in Figure 11

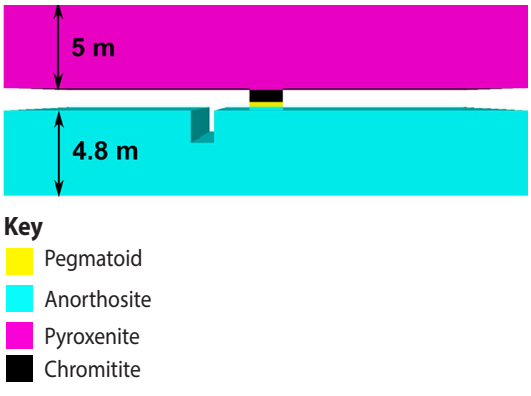

Figure 8—3D view of a model showing the hangingwall and footwall thicknesses used in the models

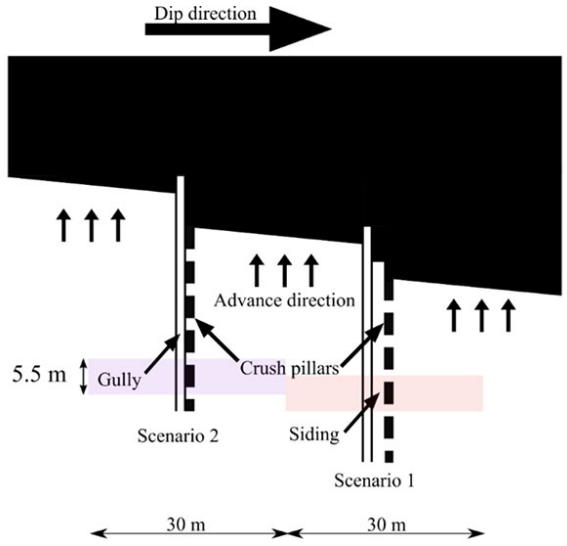

Figure 9—Schematic (plan view) showing the two modelled scenarios. The modelled areas are shown by the light-red and purple rectangles

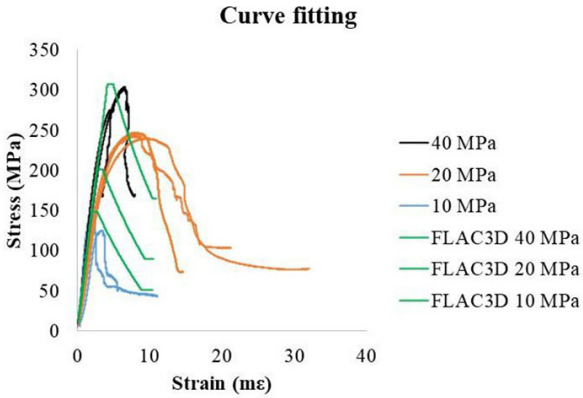

Figure 10—Curve fitting for the chromitite samples

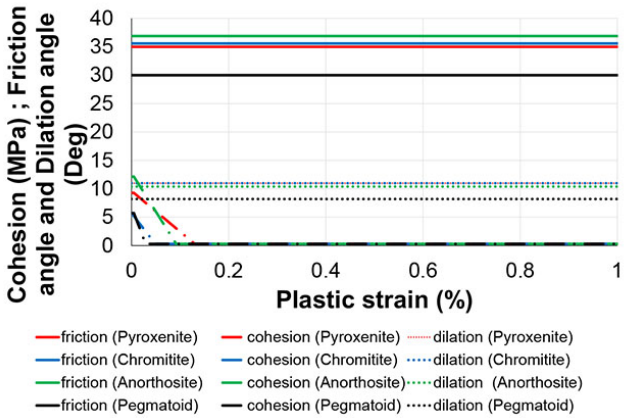

Figure 11—Strain-softening curves used in modelling pillar behaviour. The solid lines represent the friction angle, the dashed lines represent the cohesion, and the dotted lines represent the dilation angle

for the different rock types. The solid lines represent the friction angle, the dashed lines represent the cohesion, and the dotted lines represent the dilation angle.

Watson et al. (2008) found a relationship between element size and brittleness in FLAC models. Fractures develop more easily in a model with a finer grid. The research showed that brittle models were weaker than comparatively more ductile materials (Watson et al., 2008). It was therefore necessary to conduct a sensitivity

analysis on strength as a function of element size for this research. The results are shown together with model run time in Figure 12. Clearly, there is a linear relationship between stress and grid size. The most appropriate compromise on grid size between accuracy and run-time was a length of 0.100 m, a width of 0.050 m, and height of 0.0325 m, shown as unity in Figure 12. There was only about 7 MPa difference between an infinitesimal grid size and the grid that was used. This difference is within the chromitite range of UCS strength determined in a test laboratory (Watson et al., 2021a).

Scenario 1

Scenario 1 represents a case where a 2 m siding is present between the gully and the pillar. Sidings are used to change the fracture patterns resulting from high face stress and to protect people from falling rocks by having some distance (1–2.5 m) between the crush pillars and the gully, which is used as a travelling way (Du Plessis and Malan, 2018). Figure 13(a) shows the configuration of Scenario 1. The result of the model estimates a peak and residual pillar strength of 55 MPa and 9 MPa, respectively.

Figure 13(b) shows the modelled failure progression through the pillar, while Figure 13(c) shows the variation of stress as the pillar fails. Pillar failure initiated at the edges of the pillar and progressed towards the core. The stress at the pillar edge was exacerbated by the bending of strata around the pillar, causing the so-called draping effect (Watson, 2010). As the pillar approached peak strength, high stress concentrated in the core of the pillar. Confinement was provided by the frictional drag of the foundations and the draping effect. At this stage, significant damage was observed in the foundations (Figure 13(b)).

The pillar enters the post-peak phase when peak strength is exceeded, and load shedding initiates. In the post-peak phase, the average stress in the pillar reduces as the pillar approaches residual strength (Figure 13(c)). The extent of damage in the foundations is also observed to increase as the pillar approaches residual strength (Figure 13(b)). At residual strength, little further damage progression is observed. The stress concentration in the pillar is at its lowest, because its peak strength has been exceeded.

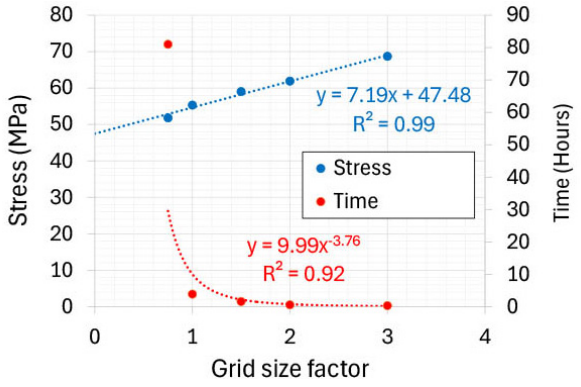

Figure 12—Effects of grid size on strength and model run time

Scenario 2

Scenario 2 represented a condition where no siding was left between the pillar and the gully, as shown in Figure 14(a). The adjacent gully changes the pillar height on one side, effectively increasing the overall pillar height. This, in turn, reduces the effective w/h ratio, making the pillar weaker. The model results estimate a peak strength of 46 MPa and a residual strength of 9 MPa (Figure 14(b)). The peak strength of Scenario 2 is significantly lower than that of Scenario 1.

Evidence of draping can be seen in the early stages of pillar deformation (Figure 14(c)), as the edges of the pillar were under high stress while the core was at low levels of stress. In Scenario 2, the progression of damage was more concentrated in the footwall. This was probably caused by the lack of confinement due to the presence of the gully. Hangingwall damage was observed, but not to the extent of the footwall.

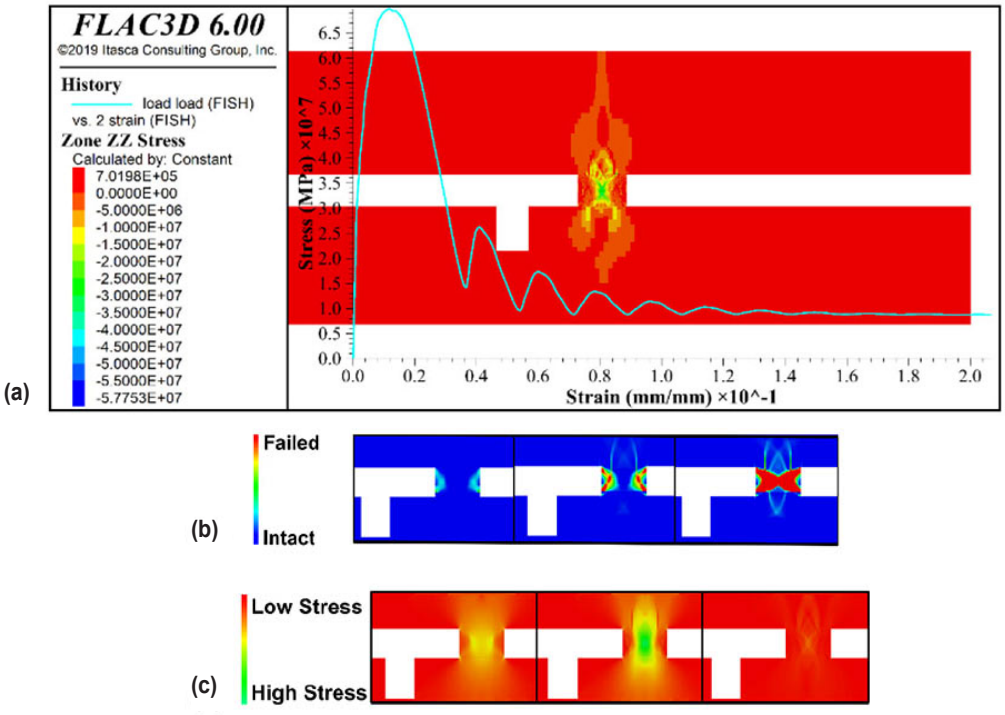

Figure 13—Model results for scenario 1 showing (a) pillar stress-strain curve, (b) progression of pillar failure (shown by the contours of plastic shear strain), and (c) variation of ZZ (vertical) stress for three stages from pillar edge failure to residual strength

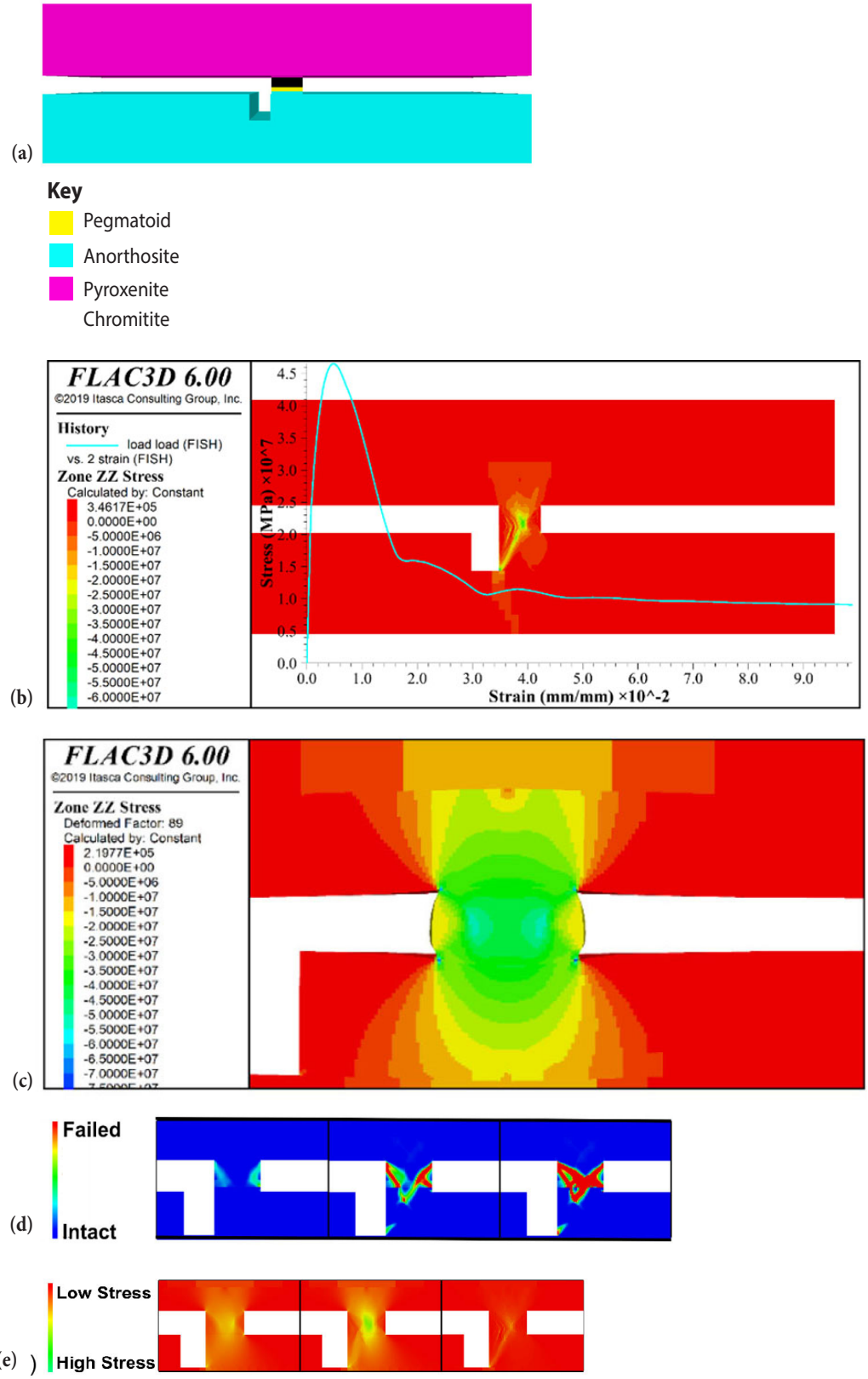

Figure 14—Model results for Scenario 2, showing (a) model setup, (b) model results, (c) draping effect, (d) progression of failure (shown by the contours of plastic shear strain), and (e) stress variation

The failure progression pattern was similar to Scenario 1 in the early stages of deformation. The pillar failure initiates from the edges of the pillar and progresses towards the core. As the stress levels approached peak, more 'failure' was observed in the footwall progressing towards the gully (Figure 14(d)). In the post-peak region, once the pillar reached residual strength, very little change in stress was observed (Figure 14(e)). The stress was high in the core of the pillar as the load approached peak strength. In the post-peak

region, the stress level dropped gradually until it reached residual strength. The deformation and failure distribution suggest that the pillar would fail into the gully.

Discussion

The modelling suggests that where a 2 m wide siding was left, the gully had little effect on the pre-peak pillar behaviour (Figure 13(b)). However, in post-failure, damage to the material in the siding was observed. This is probably due to the lack of confinement and frictional drag as the failed pillar dilated into the gully. Where no siding was left between the pillar and the gully, it was observed that the gully excavation significantly affected pillar behaviour (Figure 14(d)). Curved fractures appear to have developed at an early stage of loading from the narrower side of the pillar towards the bottom of the gully. Such fractures have also been observed underground (Watson et al., 2009).

The common empirical pillar strength formulae do not account for rectangular-shaped pillars. However, Wagner (1974) developed the 'perimeter rule' for converting rectangular pillars to square pillars, where W is the width and *L* is the length:

$$W_e \approx \frac{2WL}{(W+L)}. \quad [4]$$

Using Wagner's rule, the 4 m × 2 m pillars were 'converted' to an equivalent square pillar of 2.7 m × 2.7 m. At a stoping height of 1.3 m, the pillars with a siding have an effective w/h ratio of 2.1. The commonly used formula for pillar strength design on the UG2 Reef is a modified version of the Hedley and Grant (1972) formula, with the initial *k* value set to 35 MPa (Malan and Napier, 2011):

$$\text{Strength}_{(\text{MPa})} = 35\frac{w_e^{0.5}}{h^{0.75}}. \quad [5]$$

The modified formula predicts a strength of 46.9 MPa for the pillars with a siding, which is lower than the 55 MPa shown by the model when a GSI value of 60 was used (Hedley and Grant in Figure 15). The PlatMine formula suggests a strength of 119.8 MPa (Equation [6]), which is significantly stronger than predicted by this model (PlatMine 1 in Figure 15). A comparison between the calculated and various modelling results is provided in Figure 15.

$$\text{Strength(MPa)} = 67\frac{2.7^{0.67}}{1.3^{0.32}} = 119.8. \quad [6]$$

The planned pillar heights at the Impala operations fall slightly outside the range of the PlatMine database for UG2 pillar strengths (Watson et al., 2021). Therefore, a strength prediction was calculated assuming a pillar height within the range of the database, but at the same w/h ratio as the Impala pillars. A height of 1.5 m was used in the formula and a strength of 128.3 MPa was calculated (PlatMine 2 in Figure 15). Subsequently, further models were run with the same input parameters, but the GSI was varied to see the effect of GSI on the modelled strength.

The numerical results suggest that the pillars are stronger than predicted by the traditional modified Hedley and Grant (Malan and Napier, 2011) formula, and this has been confirmed by several researchers (Oates and Malan, 2023; Rajpal, 2012). The GSI value of 60, which was provided by the mine, may be low, because other mines have suggested higher values. A value of 70 was estimated for the Booysendal instrumentation site (Watson et al., 2021). The pillar strength predicted by the PlatMine formula (Watson et al., 2021) may be considered high for the pillars at Impala when compared with the models. Importantly though, the calculated strength was lower than predicted by the model without GSI manipulation (GSI = 100). It is recommended that underground measurements be done to verify the numerical results.

The novelty of the research described in this paper is in the use of laboratory tests to determine both peak and residual strengths of the pillar and foundation materials. The post-failure behaviour of the laboratory samples was used to establish material properties that simulated pillar behaviour as failure progressed through the pillars. It was impossible to use visual or underground measurements to calibrate the models because the research aim was to determine the depth at which crush pillars could be introduced. At the time of modelling, these pillars were not available for observations or instrumentation. The models were therefore confirmed using the PlatMine formula (Watson et al., 2021a), which was developed using observations made on other similar Bushveld mines. An instrumented pillar on the eastern side of the Bushveld Complex was used to confirm the PlatMine formula (Watson et al., 2021b), and the results are compared with the FLAC3D model without a GSI downrating in Figure 16.

Conclusions and recommendations

The investigation aimed to estimate the peak and residual strength of the planned 4 m × 2 m UG2 pillars at the Impala operations. FLAC3D models with MCSS were calibrated using laboratory tests with post-failure behaviour and employed in the strength evaluation. Some practical guides into the methodology of conducting tests on rock samples in post-failure were developed during the programme, as described in the paper. The modelled pillar height was 1.3 m, which effectively created pillars at a w/h ratio of 2. The mine typically uses an average GSI value of 60, which was adopted for the strength modelling. The models provided insights into the effects of grid size on predicted strength and

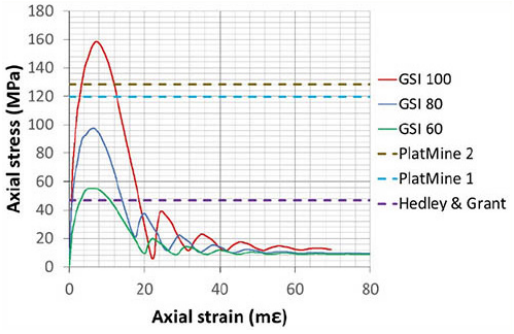

Figure 15—Comparison between the FLAC3D model with GSI values of 60, 80, and 100, the Platmine formula (Watson etal., 2021) and the modified Hedley and Grant formula (Malan and Napier, 2011)

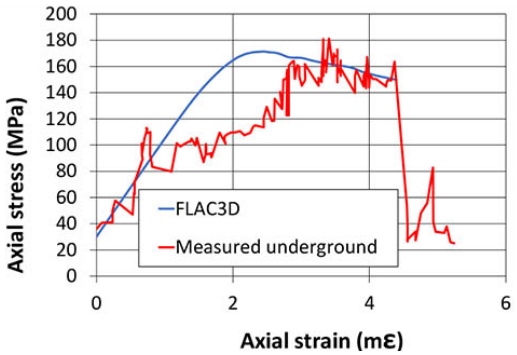

Figure 16— Comparison between the FLAC3D model without a GSI and downrating instrumentation results at Booysendal Platinum Mine (Watson 2021b)

the progression of failure through the pillars and foundations as the applied stress was increased. The most suitable grid size was established and used in all subsequent analyses. The findings of the models where a GSI of 60 was used were:

- crush pillars with sidings had peak and residual strengths of 55 MPa and 9 MPa, respectively;
- crush pillars without sidings had peak and residual strengths of 45 MPa and 9 MPa, respectively.

Subsequent analyses on the effect of GSI suggested that a value of 60 may have been too low. The results of several GSI values were compared with the modified Hedley and Grant formula with the *k*-value set at 35 MPa (Malan and Napier, 2011) and the PlatMine formula (Watson et al., 2021). The modified Hedley and Grant (Malan and Napier, 2011) formula underestimated the strengths suggested by the modelling. It could be argued that the PlatMine formula (Watson et al., 2021) overestimated the strength. However, it is important to note that the PlatMine formula strength was lower than predicted by the model without manipulated material strengths (GSI = 100). The novelty of the research was the use of laboratory tests with post-failure measurements to determine input parameters for the FLAC3D modelling. It is recommended that further underground measurements be carried out at Impala to verify the modelling results.

References

Carollo, L., 2022 Pers. comm.

Cook, N.G.W. 1963. The basic mechanics of rockbursts. *Journal of the Southern African Institute of Mining and Metallurgy*, vol. 64, pp. 11–25.

Du Plessis, M. 2015. The design and behaviour of crush pillars on the Merensky Reef (Doctoral Dissertation). University of Pretoria, Pretoria.

Du Plessis, M., Malan, D.F. 2018. Mining with crush pillars. *Journal of the Southern African Institute of Mining and Metallurgy*, vol. 118, pp. 211–216. https://doi.org/10.17159/2411-9717/2018/v118n3a3

Gardner, L.J. 2022. Pers. Comm.

Gardner, L.J., Bosman J.D. 2014. Correlation of point load index with uniaxial compressive strength for Bushveld Complex rocks. *Sixth South African Rock Engineering Symposium, SARES 2014*, Southern African Institute of Mining and Metallurgy, Johannesburg.

Ghazvinian, E., Garza-Cruz, T., Bouzeran, L., Fuenzalida, M., Cheng, Z., Cancino, C., Pierce, M. 2020. Theory and implementation of the Itasca constitutive model for advanced strain softening (IMASS). *Proceedings Eighth International Conference & Exhibition on Mass Mining*, Virtual Conference, Santiago. pp. 451–461.

Hajiabdolmajid, V., Kaiser, P.K., Martin, C.D. 2002. Modelling brittle failure of rock. *International Journal of Rock Mechanics and Mining Sciences*, vol. 39, no. 6, pp. 731–741.

Hedley, D.G.F., Grant, F. 1972. Stope pillar design for the Elliot Lake uranium mines. *Bulletin of the Canadian Institute of Mining and Metallurgy*, vol. 65, pp. 37–44.

Hoek, E. 1994. Strength of rock and rock masses. *International Society Rock Mechanics News Journal*, vol. 2, pp. 4–16.

Hudson, J.A., Crouch, S.L., Fairhurst, C. 1972. Soft, stiff and servo-controlled testing machines: a review with reference to rock failure. *Engineering Geology*, vol. 6, pp. 155–189.

Impala Mine Rock Engineering Department. 2017. Mandatory code of practice to combat rock fall and rock burst accidents in tabular metalliferous mines (Impala Platinum Limited) (No. 10.34.00.00).

Itasca. 2023. Guide to the FLAC3D documentation — FLAC3D 7.0 documentation [WWW Document]. Guide to the FLAC3D Documentation. [Online] Available at: https://docs.itascacg.com/flac3d700/flac3d/docproject/source/modeling/introduction/guidetohelp.html [accessed 10.22.23].

Jaeger, J.C., Cook, N.G.W. 1979. *Fundamentals of Rock Mechanics*, 3rd Edition, Chapman and Hall, London.

Le Bron, K.B., Gardner, L.J., van Zyl, J. 2024. A hybrid approach to pillar design: integrating empirical, strain criterion, and stress inversion concepts. *Journal of the Southern African Institute of Mining and Metallurgy*, vol. 118, pp. 211–216.

Malan, D.F., Napier, J.A.L. 2011. The design of stable pillars in the Bushveld Complex mines: A problem solved? *Journal of the South African Institute of Mining and Metallurgy*, vol. 111, pp. 821–836.

McLachlan, K. 2021. What weakens one PGM miner strengthens the rest. Moneyweb. [Online] Available at:

https://www.moneyweb.co.za/moneyweb-opinion/columnists/what-weakens-one-pgm-miner-strengthens-the-rest/ [accessed 1.22.24].

Oates, T.E., Malan, D.F. 2023. A study of UG2 pillar strength using a new pillar database. *Journal of the Southern African Institute of Mining and Metallurgy*, vol. 123, no. 5, pp. 265–274.

Oniyide, G. 2015. Thermo-mechanical behaviour of rocks from the Bushveld Igneous Complex with relevance to deeper mining, PhD thesis, School of Mining Engineering, University of Witwatersrand, Johannesburg, RSA.

Ozbay, M.U., Ryder, J.A., Jager, A.J. 1995. The design of pillar systems as practised in shallow hard-rock tabular mines in South Africa. *Journal of the Southern African Institute of Mining and Metallurgy*, vol. 4, pp. 12–30.

Rajpal, Y. 2012. Towards an improved pillar design methodology at Bathopele Mine. *Proceedings of the Southern African Institute of Mining and Metallurgy Platinum Symposium* 2012, Southern African Institute of Mining and Metallurgy, Johannesburg. pp. 483–499

RocLab, 2007. User's Guide. [online] Available at: <https://www.rocscience.com>. [Accessed 4 Jan. 2021]

Salamon, M.D.G. 1970. Stability, instability and design of pillar workings. *International Journal of Rock Mechanics and Mining Sciences*, vol. 7, pp. 613–631.

Ryder, J.A., Jager, A.J. 2002. *Rock Mechanics for Underground Mining* (2nd ed.). The Safety in Mines Research Advisory Committee (SIMRAC), Johannesburg.

Ulusay, R., Hudson, J.A. 2007. *The Complete ISRM Suggested Methods for Rock Characterization, Testing and Monitoring.* International Society for Rock Mechancs and Turkish National Group of ISRM, Ankara, Turkey. pp. 1974–2006.

Vogler, U.W.O.L. 2014. Evaluation of stiff testing of rock, MSc dissertation, School of Mining Engineering, University of Witwatersrand, Johannesburg, RSA.

Wagner, H. 1974. Determination of the complete load-deformation characteristics of coal pillars. *Proceedings of the 3rd International Congress on Rock Mechanics*, Denver, CO. Vol. 2B. International Society for Rock Mechanics, Lisbon. pp. 1076–1082.

Watson, B.P. 2010. Rock behaviour of the Bushveld Merensky Reef and the design of crush pillars, PhD thesis, School of Mining Engineering, University of Witwatersrand, Johannesburg, RSA.

Watson, B.P., Ryder, J.A., Kataka, M.O., Kuijpers, J.S., Leteane, F.P. 2008. Merensky pillar strength formulae based on back-analysis of pillar failures at Impala Platinum. *Journal of the Southern African Institute of Mining and Metallurgy*, vol.108, pp. 449–461.

Watson, B.P., Kuijpers, J.S., Miovsky, P. 2009. In situ measurements of Merensky pillar behaviour at Impala Platinum. *Journal of the Southern African Institute of Mining and Metallurgy*, vol. 109, pp. 745–754.

Watson, B.P., Kuijpers, J.S., Stacey, T.R. 2010. Design of Merensky Reef crush pillars. *Journal of the Southern African Institute of Mining and Metallurgy*, vol. 110, pp. 581–598.

Watson, B.P., Lamos, R.A., Roberts, D.P. 2021a. PlatMine pillar strength formula for the UG2 Reef. *Journal of the Southern African Institute of Mining and Metallurgy*, vol. 121, pp. 437–448.

Watson, B.P., Theron, W., Fernandes, N., Kekana, W.O., Mahlangu, M.P., Betz, G., Carpede, A. 2021b. UG2 pillar strength: verification of the PlatMine formula. *Journal of the Southern African Institute of Mining and Metallurgy*, vol. 121, no. 8, pp. 449–456.

Wawersik, W.R., Fairhurst, C. 1970. A study of brittle rock fracture in laboratory compression experiments. *International Journal of Rock Mechanics and Mining Sciences and Geomechanics Abstracts*, vol. 7, pp. 561–575. ◆